Fermi National Accelerator Laboratory

Target Systems Department

Accelerator Division

Analytical & Experimental Study of Radio Frequency Cavity Beam Profile Monitor

Author:
Mario D. Balcazar

Supervisor:
Katsuya Yonehara

October 22, 2017

CONTENTS

I. Abstract 3

II. Introduction 3

III. Beam Distribution Analysis 3
A. Beam parameters 4
B. Target parameters 4
C. Radiation length 5
D. Multiple scattering 6
E. Beam size 6

IV. Hadron Monitor Configuration 8

V. Ion-Pair Production Analysis 15
A. Most Probable Energy Loss 15
B. Ion Pair Production 15

VI. Tunable Q-Factor RF Cavity 17
A. Conceptual Design 17
B. Benchtop Measurements 19

VII. Concluding Remarks 22

I. ABSTRACT

The purpose of this analytical and experimental study is multifold: 1) To explore a new, radiation-robust, hadron beam profile monitor for intense neutrino beam applications; 2) To test, demonstrate, and develop a novel gas-filled Radio-Frequency (RF) cavity to use in this monitoring system. Within this context, the first section of the study analyzes the beam distribution across the hadron monitor as well as the ion-production rate inside the RF cavity. Furthermore a more efficient pixel configuration across the hadron monitor is proposed to provide higher sensitivity to changes in beam displacement. Finally, the results of a benchtop test of the tunable quality factor RF cavity will be presented. The proposed hadron monitor configuration consists of a circular array of RF cavities located at a radial distance of $7cm$ – corresponding to the standard deviation of the beam due to scaterring – and a gas-filled RF cavity with a quality factor in the range $400 - 800$.

II. INTRODUCTION

An intense neutrino beam is a unique probe for researching beyond the standard model. Fermilab is the main institution to produce the most powerful and wide-spectrum neutrino beam. From that respective, a radiation robust beam diagnostic system is a critical element in order to maintain the quality of the neutrino beam. To this end, a novel radiation-resistive beam profile monitor based on a gas-filled RF cavity has been proposed.

Gas in the cavity serves as an ionization media by interacting with incident charged particles. The amount of beam-induced plasma is then proportional to the number of incident particles. The plasma consumes the RF power, so called plasma loading. This phenomenon is interpreted as a plasma resistance which induces the RF power dissipation in the plasma. The beam profile is reconstructed by observing the amount of plasma loading from an individual cell in a multi-RF cavity which forms a hodoscope structure.

The proposed research and development timeline for this monitoring system consists of a series of beam tests with different intensities and cavity designs. First, the apropriate quality factor (Q-factor) of the cavity will be studied by performing a table-top test with a novel tunable Q-factor RF cavity. Following this measurement the cavity will be exposed to a beam test from which the accuracy of the signal will be analyzed. A final intense beam test will be performed to evaluate the radiation robustness of the RF cavity for hadron beam profile monitoring applications.

Within this context, the presented analysis has a two-fold purpose: analitically study the beam distribution across the monitor and ion production inside the RF cavity, and present the first benchtop measurements of the tunable Q-factor RF cavity.

III. BEAM DISTRIBUTION ANALYSIS

The first section this study starts with an analysis of the hadron beam distribution across the monitor. The future RF cavity beam profile monitor follows the behavior of an ionizing chamber very similarly. In the present ion chamber of the NuMI Experiment at Fermilab, the ionized particles induce a voltage across the hadron monitor plates and this results in the generation of a signal. Similarly, in the future RF cavity monitor the ions created inside the cavity by the energetic beam will result in the reduction of the RF power.

This analysis will start by studying the distribution of the hadron beam across the NuMI Experiment hadron monitor. Using the NuMI given specifications, the multiple scattering angle of a high energetic beam will be calculated. The approximation parameters are the following: a $1m$ graphite target followed by a $\approx 700m$ Helium-filled decay pipe. The size of the beam reaching the end of the pipe can be inferred by using the scattering angle and assuming a gaussian distribution across the monitor. From this result the most effective hadron monitor configuration will be proposed.

A. Beam parameters

From the beam's initial momentum, the γ and total energy E_T parameters were calculated using relativistic relationships,

$$\gamma = \frac{E_T}{E_0} \tag{1}$$

$$E_T = \frac{p}{\beta} \tag{2}$$

The incident high-energy beam is hadronic and it has the following properties:

- $p = 120$ GeV
- $\beta = 0.99997 \approx 1$
- $\gamma = 127.9$
- $N_0 = 4 \times 10^{13}$

From this parameters, the beam has a $\beta\gamma$ product of,

$$\beta\gamma \approx 128 \tag{3}$$

B. Target parameters

The beam target is composed of a 1m long graphite surface followed by a 700m long Helium-filled decay pipe. The following properties follow from these scattering mediums:

Carbon (Graphite):

- Atomic number: $Z = 6$
- Atomic mass: $A = 12.0115$
- Density: $d_c = 2.210 \quad g/cm^3$
- Volume: $\rho_c = 200 \quad cm^3$
- Total mass: $m_c = 442 \quad g$

Helium gas:

- Atomic number: $Z = 2$
- Atomic mass: $A = 4$
- Density $d_h = 1.664 \times 10^{-4} \quad g/cm^3$
- Volume $\rho_h = 2.2 \times 10^9 \quad cm^3$
- Total mass $m_h = 366080 \quad g$

C. Radiation length

The radiation length of a high-energy particle beam is defined as the characteristic amount of matter traversed for energy loss interactions in the medium. Radiation length is commonly defined as X_0 as the mean distance over which a high-energy electron loses all but $1/e$ of its energy from bremsstrahlung. For both mediums, the graphite target and the helium decay pipe, the radiation length will be approximated by the formula shown below,

$$X_0 = \frac{(716.4)(A)}{Z(Z+1)\ln\left(\frac{287}{\sqrt{Z}}\right)} \tag{4}$$

Where A, and Z are the atomic mass and atomic number of the absorber material.

This radiation length formula, however, results in an approximated radiation length in g/cm^2 for a single material layer. Since the study involves beam scaterring through two stages composed of Graphite and Helium, equation (4) will be used in combination with the formula for the radiation length of a composite material given by,

$$\frac{1}{X_0} = \sum \frac{w_j}{X_j} \tag{5}$$

Where w_j, and X_j are the fraction by weight and the radiation length for the jth element.

It is important to note here that we are treating radiation length as a probability parameter. Because of this, a 1m carbon target has less probability of producing scattering compared to a 700m Helium pipe. Even though the individual radiation length of carbon is much higher than helium, when specific volumes are included in the calculations the probability of the combined medium results more similar to that of helium – extended over a long distance – rather than the one of carbon.

The approximate radiation length of the Graphite layer is obtained by

Carbon (Graphite):

$$\begin{aligned} X_0 &= \frac{(716.4)(A)}{Z(Z+1)\ln\left(\frac{287}{\sqrt{Z}}\right)} \\ X_c &= \frac{(716.4)(12)}{6(6+1)\ln\left(\frac{287}{\sqrt{6}}\right)} \\ X_c &\approx 42.969 \quad [g/cm^2] \end{aligned} \tag{6}$$

Similarly, the radiation length of the helium gas layer is given by,

Helium gas:

$$\begin{aligned} X_0 &= \frac{(716.4)(A)}{Z(Z+1)\ln\left(\frac{287}{\sqrt{Z}}\right)} \\ X_h &= \frac{(716.4)(4)}{2(2+1)\ln\left(\frac{287}{\sqrt{2}}\right)} \\ X_h &\approx 89.894 \quad [g/cm^2] \end{aligned} \tag{7}$$

It follows that the combined radiation length for both layers X_t, the graphite target and the helium pipe, is obtained with $Eq.(5)$

$$\begin{aligned}
\frac{1}{X_0} &= \sum \frac{w_j}{X_j} \\
\frac{1}{X_t} &= \left(1.2 \times 10^{-3}\right)\left(\frac{1}{42.969}\right) + (0.998)\left(\frac{1}{89.894}\right) \\
X_t &\approx 89.776 \quad [g/cm^2]
\end{aligned} \tag{8}$$

Finally, the total radiation length can be divided by the total density to obtain units of cm as follows,

$$\begin{aligned}
d_t &= \sum w_i d_i = w_c d_c + w_h d_h \\
d_t &= \left(\frac{442}{442 + 366080}\right)(2.210) + \left(\frac{366080}{442 + 366080}\right)\left(1.664 \times 10^{-4}\right) \\
d_t &= 2.83 \times 10^{-3} \quad [g/cm^3]
\end{aligned} \tag{9}$$

Therefore, the total radiation length can be written as

$$X_t \approx 89.776 \quad [g/cm^2] \approx 31708 \quad [cm] \tag{10}$$

D. Multiple scattering

A particle beam travessing through a medium will be deflected by small scatters, mostly resultant of Coulomb interactions from the nuclei. The net scattering and displacement of the beam through the target is described by a Gaussian distribution and the central limit theorem. These Coulomb scaterring distributions can be effectively modeled by the theory of Moliere. Defining the rms scaterring angle as,

$$\theta_0 = \theta_{plane}^{rms} \tag{11}$$

Then, the central 98% of the projected angular distribution can be decribed for many application with a Gaussian approximation given by,

$$\theta_0 = \frac{13.6MeV}{\beta cp} z \sqrt{\frac{x}{X_0}} \left(1 + 0.038 \ln\left(\frac{x}{X_0}\right)\right) \tag{12}$$

Where p, βc, and z, are the momentum, velocity, and charge number of the incident particle, and x/X_0 is the thickness of the scattering medium in radiation lengths.

From the previous calculation of the total radiation length, the scattering angle for the combined medium is,

$$\begin{aligned}
\theta_0 &= \frac{13.6MeV}{\beta cp} z \sqrt{\frac{x}{X_0}} \left(1 + 0.038 \ln\left(\frac{x}{X_0}\right)\right) \\
\theta_0 &= \frac{13.6}{(1)(120 \times 10^3)}(1)\sqrt{\frac{701 \times 10^2}{31708}} \left(1 + 0.038 \ln\left(\frac{701 \times 10^2}{31708}\right)\right)
\end{aligned} \tag{13}$$

$$\theta_0 \approx 0.17 \quad [mRad]$$

E. Beam size

The initial number of protons in the beam before reaching the target was defined as $N_0 = 3 \times 10^{13}$. Nevertheless, nuclear strong interactions must also be taken into account. Nuclear interaction length is a measurement of how

many incident hadrons strongly interact with the target material. In case of graphite, the nuclear interaction length is $38.83cm$. Hadrons undergoing strong interactions usually lose their momentum and scatter away from the original beam path, this is commonly called inelastic scattering. Thus, the radiation length roughly tells the transmission of protons through the target,

$$\begin{aligned} N_p &\approx N_0 \exp^{\frac{-L}{38.8}} \\ N_p &= (4 \times 10^{13}) \exp^{\frac{-100}{38.8}} \\ N_p &= 3 \times 10^{12} \end{aligned} \tag{14}$$

Therefore, only 7.6% of the initial protons survive the graphite target. The radiation length in helium gas is sufficiently small that it will be ignored. The beam size will be obtained by assuming a Gaussian distribution. Based on the scattering angle result, the vertical displacement of the beam is given by the small angle approximation,

$$\begin{aligned} \tan(\psi^{rms}) \approx \psi^{rms} &= \frac{y}{x} \\ y &= (\psi^{rms})(x) \\ y &= (\frac{\theta^{rms}}{\sqrt{3}})(x) \\ y &= (0.1 \times 10^{-3})(700) \\ y &= 0.07 \quad [m] \\ y &= 7 \quad [cm] \end{aligned} \tag{15}$$

In other words, the beam will be deviated at approximately $7cm$ from the center of target in both the x and y directions. Note that based on the multiple scattering approximation this distance corresponds to the standard deviation σ of the beam distribution across the target. This relationship will play a major role during the hadron monitor configuration in the next section.

Assuming a mean $\mu = 0$ and a central detector of dimensions $0.05x0.05m$ the percentage of protons k reaching the central pixel of the final detector can be computed as follows,

$$\begin{aligned} k &= \int_{-5}^{5} \frac{1}{\sigma\sqrt{2\pi}} \exp^{-\frac{(x-\mu)^2}{2\sigma^2}} \\ k &= \int_{-5}^{5} \frac{1}{(7)\sqrt{2\pi}} \exp^{-\frac{(x)^2}{2(7)^2}} \\ k &= 0.52\% \end{aligned} \tag{16}$$

In other words, from the 3×10^{12} protons that survived the carbon target, 0.52% of them are located within the $5 \quad cm^2$ of the central pixel. Thus, the number of photons reaching the central pixel is

$$\begin{aligned} N &= (0.52)(N_p) \\ N &= (0.52)(3 \times 10^{12}) \\ N &= 1.58 \times 10^{12} \end{aligned} \tag{17}$$

IV. HADRON MONITOR CONFIGURATION

The correspondance of the scaterring angle to the standard deviation σ of the beam distribution has an important implication. Let's consider the standard 1-dimensional Gaussian distribution of the beam reaching the monitor,

$$f(x) = y = \frac{1}{\sigma\sqrt{2\pi}} e^{-\frac{(x-\mu)^2}{2\sigma^2}} \tag{18}$$

In this case, x is the physical location of the incident particle with respect to the center of the monitor, μ then is the mean distance 0 (namely the center of the monitor), and y is the probability that such particle will hit that distance x from the center.

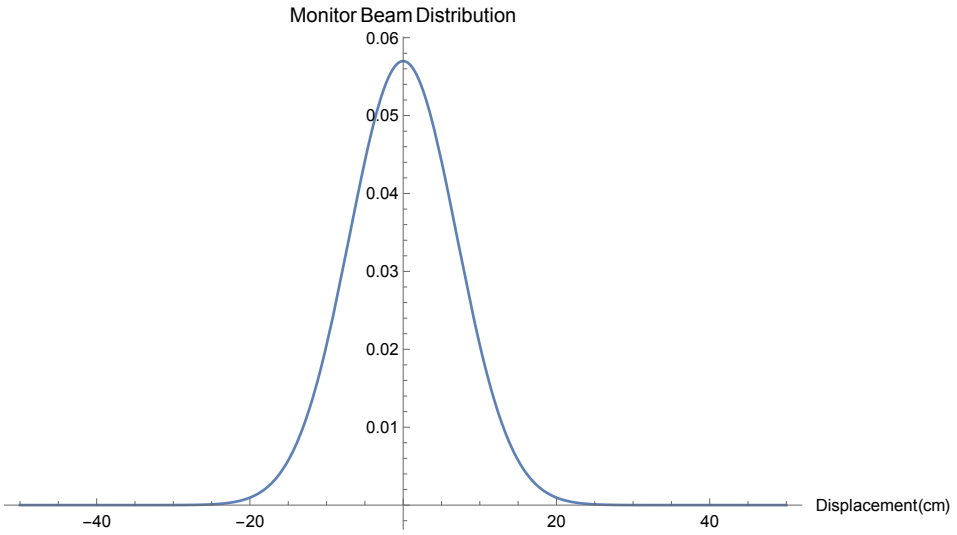

Figure 1. 1-Dimensional Beam normal distribution of hadron beam hitting the monitor target.

Note that since all the area of the monitor is homogeneous, the probability of a particle hitting the monitor is the same across its area at any location x. This means that the only external factor affecting the probability of a particle hitting the monitor is the number of beam particles hitting that location. We can then say that in the normal distribution of the beam across the monitor, y is the 'intensity' of the beam at the location x.

Directly from that conclusion, dy/dx is the change of intensity with respect to a change in displacement of the beam. In other words, the absolute value of dy/dx provides the equation for the *sensitivity of the monitor as a function of displacement*. It relates the change of intensity in the monitor to a change in position. Assuming a mean $\mu = 0$ equal to zero at center of the monitor it follows,

$$\frac{\partial y}{\partial x} = -\frac{1}{\sigma\sqrt{2\pi}} \left(\frac{x}{\sigma^2}\right) e^{-\frac{x^2}{2\sigma^2}} \tag{19}$$

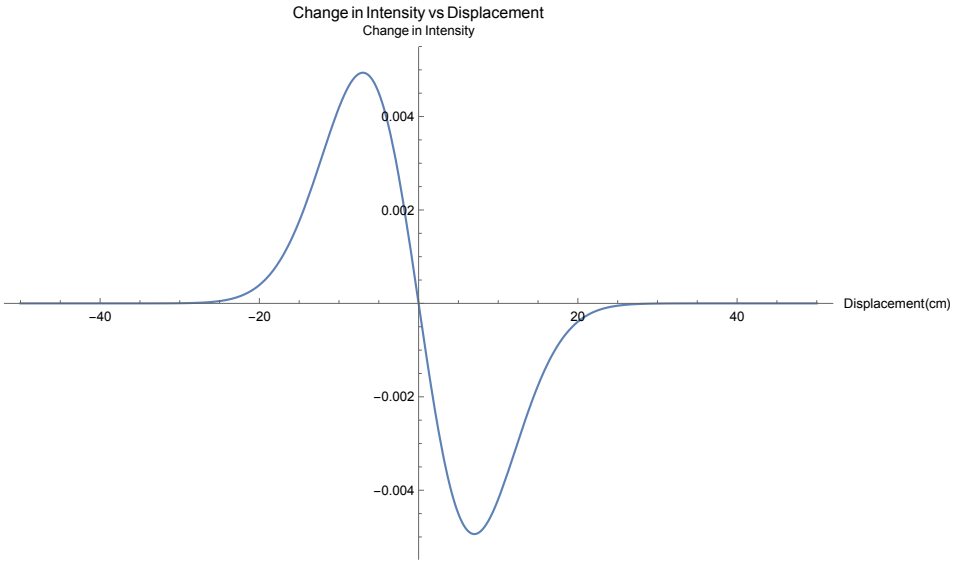

Figure 2. Plot of the derivative of the beam distribution. It shows the rate of change in intensity across the monitor as a function of displacement.

The change in 'intensity' of detection with respect to position is critical to stablish the beam profile. Since the size of the pixels (or RF cavities) is much larger than the average physical displacement of the beam, the most appropriate way to detect a change in beam displacement is to detect a change in beam intensities. Furthermore, in order to obtain the most sensitive position of the monitor at which a change of 'intensity' y with respect to a change in position x reaches a maximum values, the derivative dy/dx must be taken twice. Then, if we wish to find the point at which the change in 'intensity' is the **greatest** for a change in position x, then d^2y/dx^2 must be set equal to zero.

$$\begin{aligned} -\frac{1}{\sigma\sqrt{2\pi}}\left(\frac{1}{\sigma^2}\right)e^{-\frac{x^2}{2\sigma^2}} + \frac{1}{\sigma\sqrt{2\pi}}\left(\frac{x^2}{\sigma^4}\right)e^{-\frac{x^2}{2\sigma^2}} &= 0 \\ \frac{1}{\sigma\sqrt{2\pi}}\left(\frac{1}{\sigma^2}\right)e^{-\frac{x^2}{2\sigma^2}} &= \frac{1}{\sigma\sqrt{2\pi}}\left(\frac{x^2}{\sigma^4}\right)e^{-\frac{x^2}{2\sigma^2}} \\ \therefore x &= \pm\sigma \end{aligned} \tag{20}$$

This means that at position $x = \sigma$ the hadron monitor is the most sensitive to a change in displacement. This can be confirmed by observing the plot of the absolute value of dy/dx. This graph presents 'sensitivity as a function of displacement'.

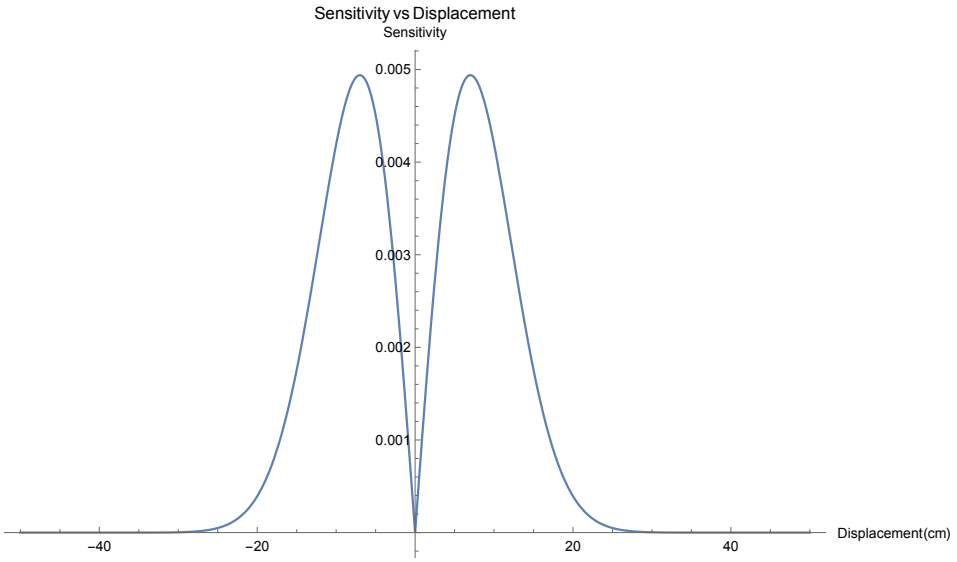

Figure 3. Plot of the absolute value of the derivative of the beam distribution. It shows the maximum sensitivity across the monitor as a function of beam displacement.

Based on this realization, a more efficient pixel configuration can be designed across the hadron monitor such that it is highly sensitive to a change in the beam displacement. Based on the previous calculations of the beam distribution and sensitivity let's now consider a 3-Dimensional plot of the beam reaching the hadron monitor.

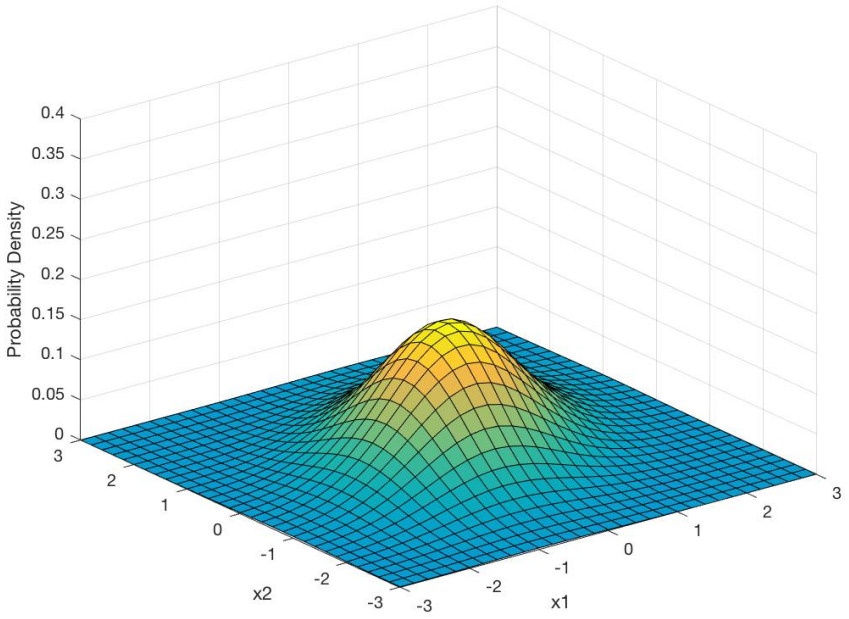

Figure 4. Beam distribution across the beam profile monitor.

A change in the displacement of the beam would result in a change in the number of particles hitting the monitor at all locations. This change in intensity will be best measured if the pixels are located at the most sensitive point across the beam distrbution. This point will correspond to the location in the monitor at which a change in the number of hitting particles will result in the greatest **difference**.

For example, since the center of monitor receives the greatest number of particles, a change in this number by a

small difference (small beam displacement) will not result in a big change in the net number of particles hitting that location (intensity). The same is true for the tail of the distibution. Based on the previous calculations, the most sensitive location to a change in beam intensity is exactly the location of the standard deviation σ that was obtained with the scatterring angle calculation. A 3-Dimensional plot of the sensitivity of the monitor to a change in beam displacement is shown below.

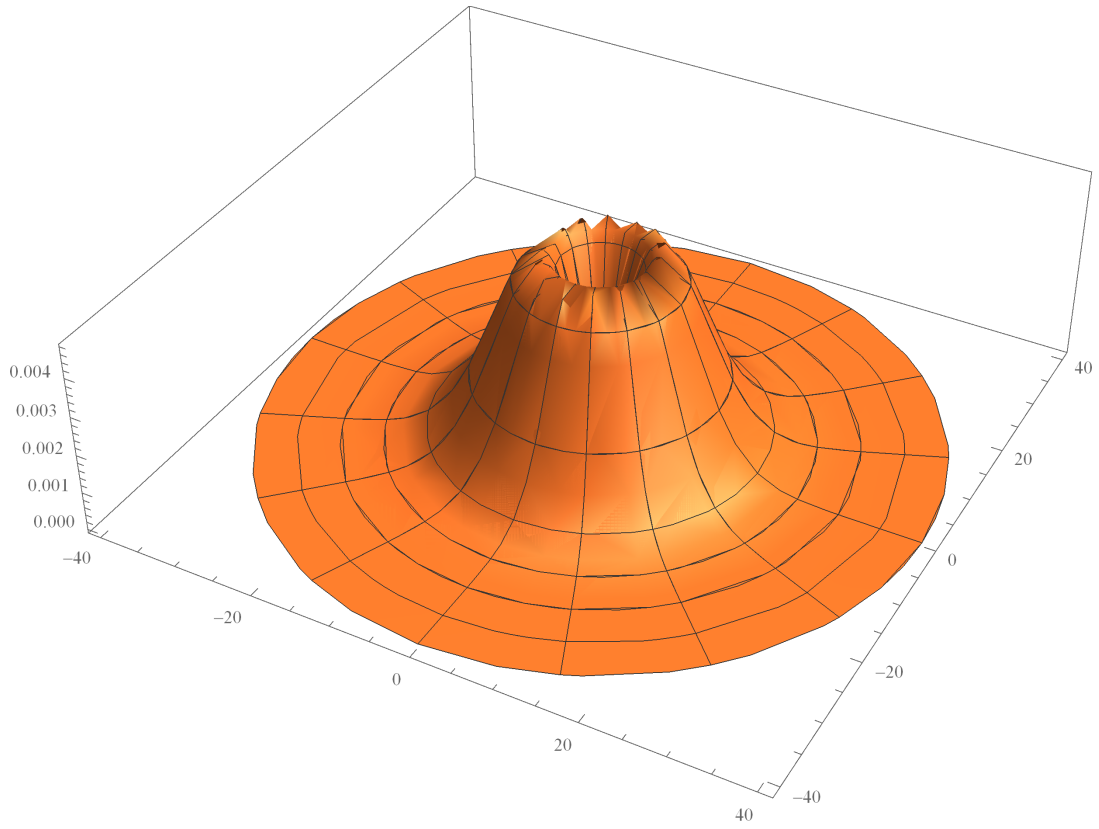

Figure 5. 3-Dimensional distribution of sensitivity across the monitor to a change in the beam displacement.

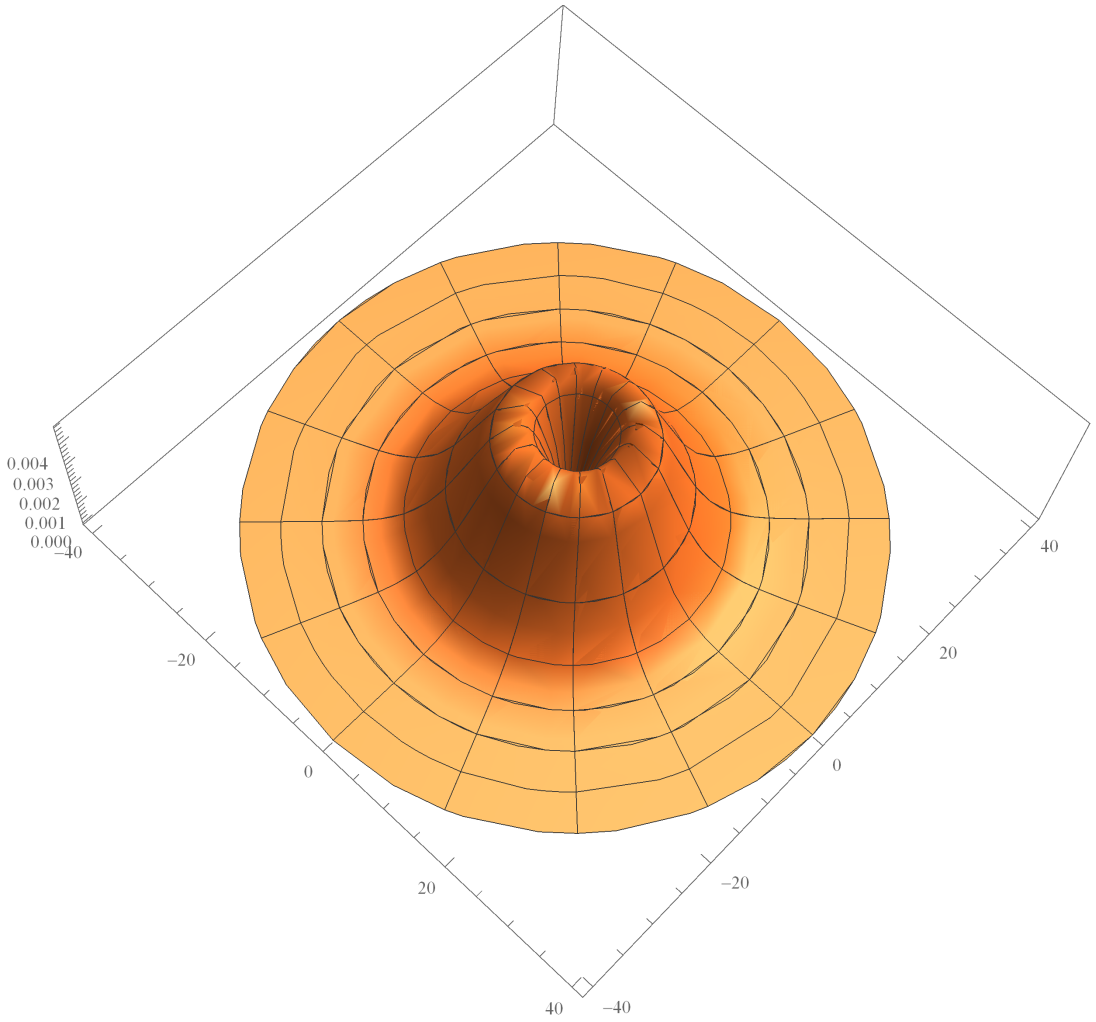

Figure 6. 3-Dimensional distribution of sensitivity across the monitor to a change in the beam displacement.

Therefore, a "doughnut" pixel configuration will then result in the greatest sensitivity to beam displacements. This leads to the final stage of the initial RF Cavity Hadron monitor design. Two designs are proposed in this study. In the first design a center RF cavity is located in the middle of the monitor and it is surrounded by a sectional cavities forming a toroidal structure. In the second design, 5 RF cavities are used including one in the center and 4 around it centered at the sensitive locations of the monitor. An initial illustration of both of this hadron monitor configurations based on sensitivity are presented below. The pixel positions contour of maximum sensitivity is marked by a white line in the figures.

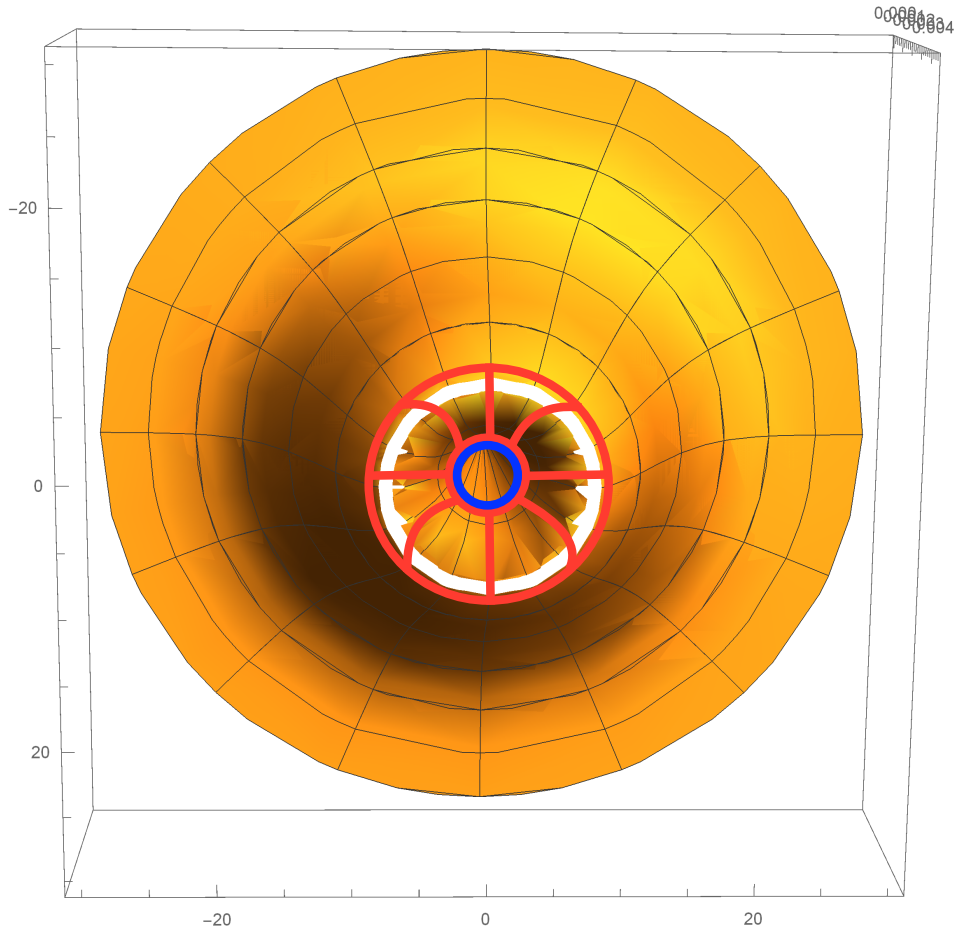

Figure 7. First RF cavities configuration across beam profile monitor based on sensitivity.

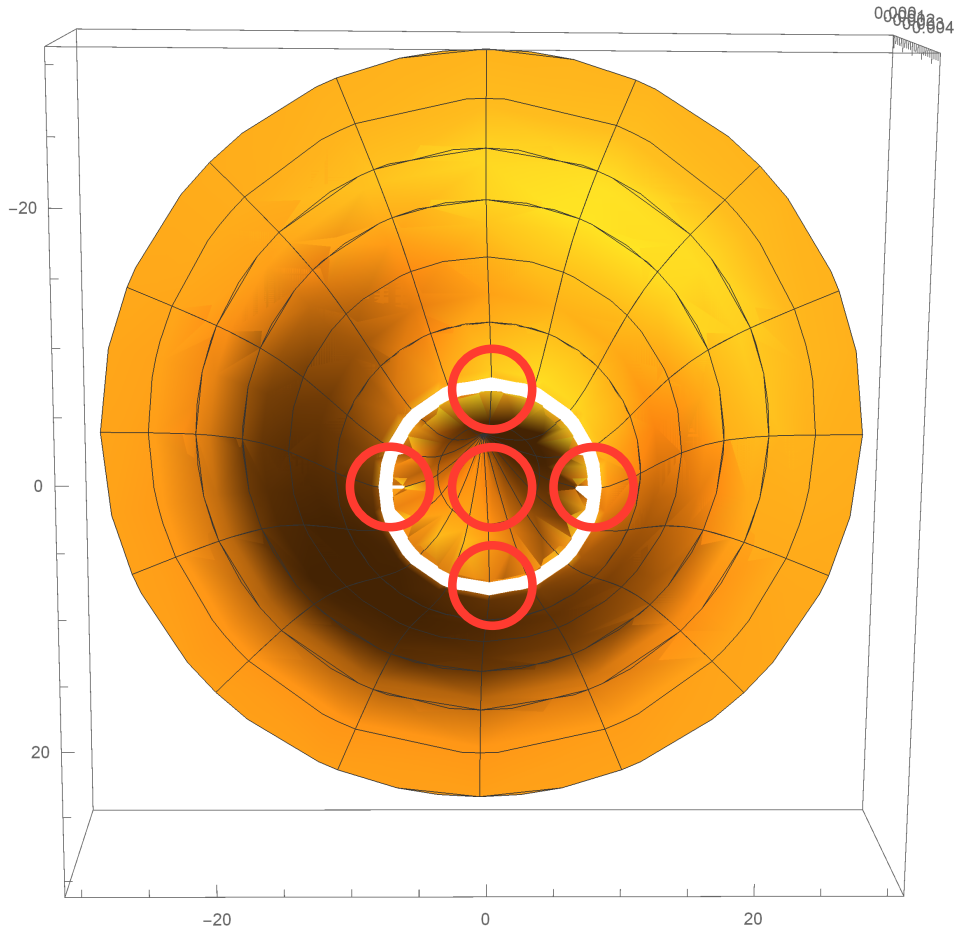

Figure 8. Second RF cavities configuration across beam profile monitor based on sensitivity.

V. ION-PAIR PRODUCTION ANALYSIS

The second section of the analytical analysis involves an estimation of the ion-pair production and induced voltage inside a particle beam ionizing chamber. The beam of particles incident to the gas-filled RF cavity monitor will result in the creation of ions. This plasma ions will have the effect of a load inside the cavity, thus reducing its RF power. The following part of the analysis focuses on the number of ions created inside the cavity due to incident protons beam.

A. Most Probable Energy Loss

The Bethe equation commonly used to calculate energy loss is weighted by very rare events with large single-collisions energy deposits. Far better and more easily measured is the most probable energy loss described by the Landau distribution. The most probable energy loss in a detector is considerably below the mean given by the Bethe equation. For detectors of moderate thickness, the Landau's most probable energy loss probability distribution of a single particle is

$$\Delta p = \xi \left[\ln\left(\frac{2mc^2\beta^2\gamma^2}{I}\right) + \ln\left(\frac{\xi}{I}\right) + j - \beta^2 - \delta(\beta\gamma) \right] \tag{21}$$

Where, $\xi = (K/2)\langle Z/A\rangle(x/\beta^2)MeV = 6.387 \times 10^{-7} \quad MeV$. The high-energy behavior of particles is such that $\Delta E \approx \Delta p$ and so for $\beta\gamma \geq 100$,

$$\begin{aligned} \Delta p \longrightarrow & \left[\ln\left(\frac{2mc^2\xi}{(\hbar\omega_p)^2}\right) + j \right] \\ & = (6.387 \times 10^{-7}) \left[\ln\left(\frac{2(0.511)(6.387 \times 10^{-7})}{(0.26 \times 10^{-6})^2}\right) + 0.2 \right] \\ & = 1.04 \times 10^{-5} \quad MeV \end{aligned} \tag{22}$$

Therefore, the Landau most probable energy loss, like the restricted energy loss, reaches a Fermi Plateu. the most probable energy loss in a detector of thickness $x = 8.32 \times 10^{-6} \quad g/cm^2$ is,

$$\frac{\Delta E}{\Delta x} \approx \frac{\Delta p}{x} = 1.251 \quad MeV cm^2 g^{-1} \tag{23}$$

Note that the mean of the energy loss given by the Bethe equation is ill-defined experimentally and is not useful for describing energy loss by single particles. It rises as $\ln(\gamma)$ because W_{max} increases γ at high energies. *The most probable energy loss should be used.*

B. Ion Pair Production

The production number of ion pairs inside the chamber can then be obtained by finding the quotient of the total amount of energy loss in the chamber divided by its ionization energy. This is,

$$n_i = \frac{\Delta E/\Delta x}{w_i} \tag{24}$$

Where n_i is the number of ion pairs produced per incident proton, $\Delta E/\Delta x$ is the amount of energy lost in the detector, and w_i is the minimum ion-pair production energy.

All that is needed has been calculated to finally compute the number of ion-pairs produced inside the ionizing chamber. Using the most probable energy loss in the detector in MeV, a mean ion production energy of $w_i = 30.6 \quad eV$, and *Eq. (28)*,

$$\begin{aligned} n_i &= \frac{\Delta E/\Delta x}{w_i} \\ &= \frac{10.4}{40.3} \\ &= 0.258 \quad ions \end{aligned} \tag{25}$$

From the previously calculated total number of incident particles N, the total number of ion-pair production is,

$$\begin{aligned} N_T &= (n_i) \times (N) \\ N_T &\approx 4 \times 10^{11} \quad ions \end{aligned} \tag{26}$$

The final step is to calculate the induced voltage inside the cavity by the ionized beam particles through the following conversion factor

$$10 \quad [nC] = 1V \tag{27}$$

From the approximated total number of ions produced inside the chamber, the resulting induced voltage is

$$V_i = \frac{(4 \times 10^{11})(1.602 \times 10^{-19})}{10 \times 10^{-9}} \tag{28}$$

Where V_i is the total induced voltage. Therefore,

$$\therefore V_i = 6.4 \quad [V] \tag{29}$$

Comparing this result with the experimental measurements taken from the NuMI experiment hadron monitor, it can be appreaciated the accuracy of the result.

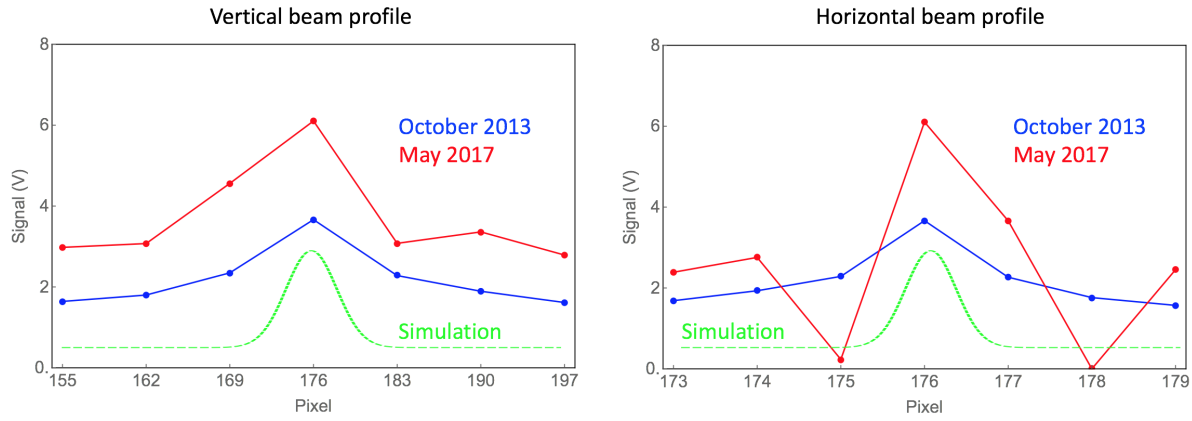

Figure 9. Pixel voltage signals across the NuMI Experiment hadron monitor.

VI. TUNABLE Q-FACTOR RF CAVITY

A. Conceptual Design

The use of a Radio-Frequency cavity as a hadron monitoring system has the potential to provide a radiation robustness technique for reconstructing the beam profile. The gas-filled RF cavity hadron monitor works by correlating the RF power loss inside the cavity (from gas ionization) to the incident beam energy. Thus, the plasma loading will be proportional to the beam intensity. Within this context, the quality factor of the cavity (Q-factor) is a key parameter to obtain a ratio between the power supplied to cavity to the power lost due to plasma loading.

High Q-factor RF cavities are commonly desired in accelerator applications since a low power supply can be used to gradually increase the energy inside the cavity without loosing power. However, the nature of high-Q cavities also prevents to quickly feed energy back into the cavity due to its large impedance. On the other hand, low Q-factor RF cavities allow to more rapidly feed power back into the cavity to compensate for energy loss. Nevertheless, low Q-factor cavities require larger supplies of power to mantain energy inside the cavity. The opposite behavior between high-Q and low-Q cavities require the development of a hadron monitoring system with a RF cavity at an intermediate quality factor. The Q-factor of the RF cavity hadron monitor needs to be high enough to guarantee the containment of RF power inside the cavity, while low enough so that power can be supplied back quickly after the beam ionization.

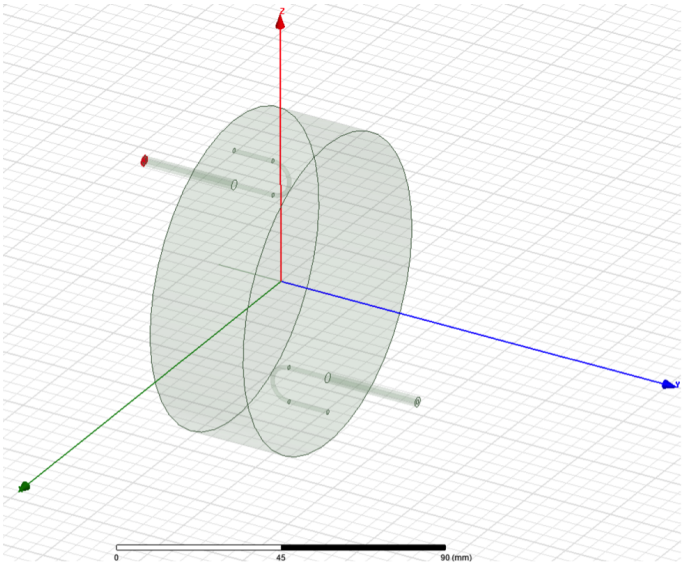

Figure 10. Design of tunable Q-factor RF pillbox cavity.

In light of this problem, an innovative approach was taken to determine the adequate quality factor of the hadron monitor RF cavity. Specifically, a tunable Q-factor RF cavity was develop to study this precise problem. Figure [1] shows the conceptual design of the tunable Q-factor RF test cavity. A main frame is a 2.45 GHz pillbox stainless steel RF cavity and two loading loops installed on the top plate to adjust the Q-factor. The Q-factor can be tuned from approximately 1,000 to 100 by rotating the loading loops and thus changing the coupling strength of the signal to the cavity. Figure [2] shows a block diagram of RF electronic system. Since the peak power of the cavity is 1 - 10 mW, a standard RF source (HP8341A + a solid-state RF amplifier) is used. In order to measure RF envelope precisely, a fast RF peak power detector (Boonton, RTP5000) will be used. The power meter has good sensitivity in the range of -50 to 20 dBm. A spectrum analyzer (E4445A) and/or network analyzer are used to measure the coupling strength of each loop and the quality factor of cavity.

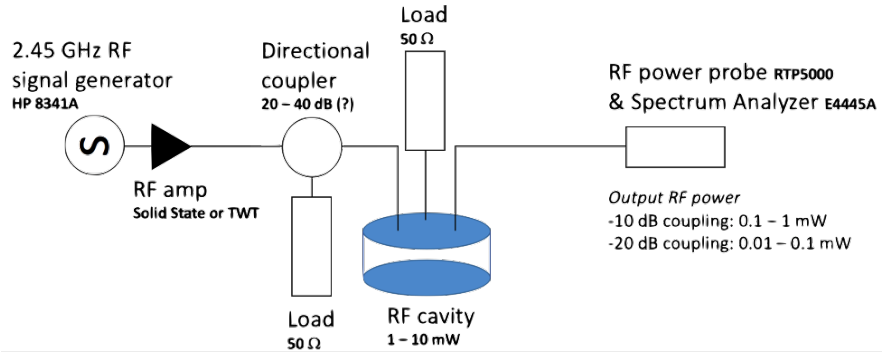

Figure 11. Electronic configuration of calibration measurements of tunable Q-factor RF cavity.

Numerical simulations for the pillbox cavity were performed on HFSS software. During these analysis it was observed that by rotation of the coupling loops inside the cavity a greater impedance was obtained obtained and the RF power decreased. The critical coupling and decoupling of the the loading loops then shows the possibility of increasing and decreasing the excitation of the TM010 resonant mode of the cavity. In essence, *power bleeding* through magnetic coupling loops is the main mechanism behind the tunability of the Q-factor inside the cavity. The images below show captures of the HFSS simulation.

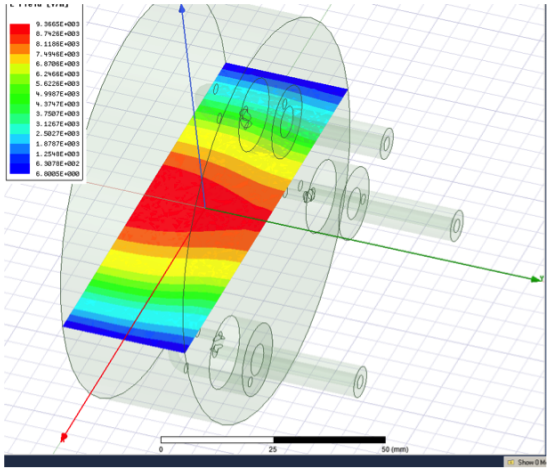

Figure 12. HFSS simulation 1 of tunable Q-factor RF cavity.

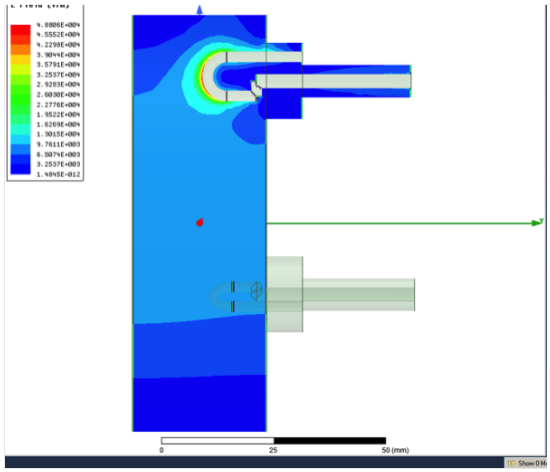

Figure 13. HFSS simulation 2 of tunable Q-factor RF cavity.

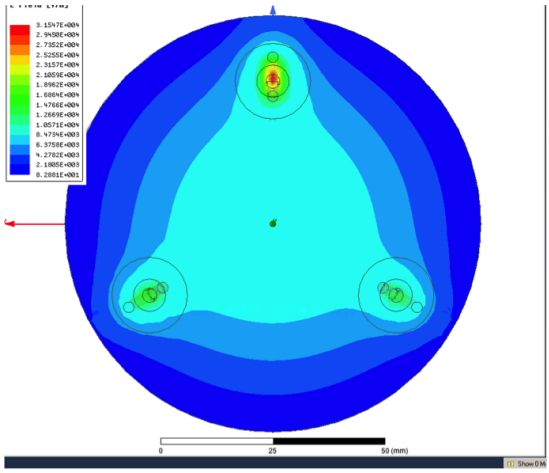

Figure 14. HFSS simulation 3 of tunable Q-factor RF cavity.

The tunable Q-factor RF cavity design was fabricated, calibrated, and tested by rotating the magnetic coupling loops. The determination of the corresponding quality factor was done with a spectrum/network analyzer by measuring bandwidth and resonant frequency. The results of these measurements are the focus of the next section.

B. Benchtop Measurements

The goal of this measurement is to use the tunable Q-factor RF test cavity described in the previous section to study the accuracy of the RF signal as a function of the Q-factor. Measurement error in the RF calibration is particularly investigated in order to improve the RF cavity design. The tunable Q-factor cavity will also be used in future beam tests in which the electron capture time will be measured as functions of Q-factor and concentration of electronegative dopant. Figure [] shows a physical image of the tunable Q-factor used in the benchtop measurements.

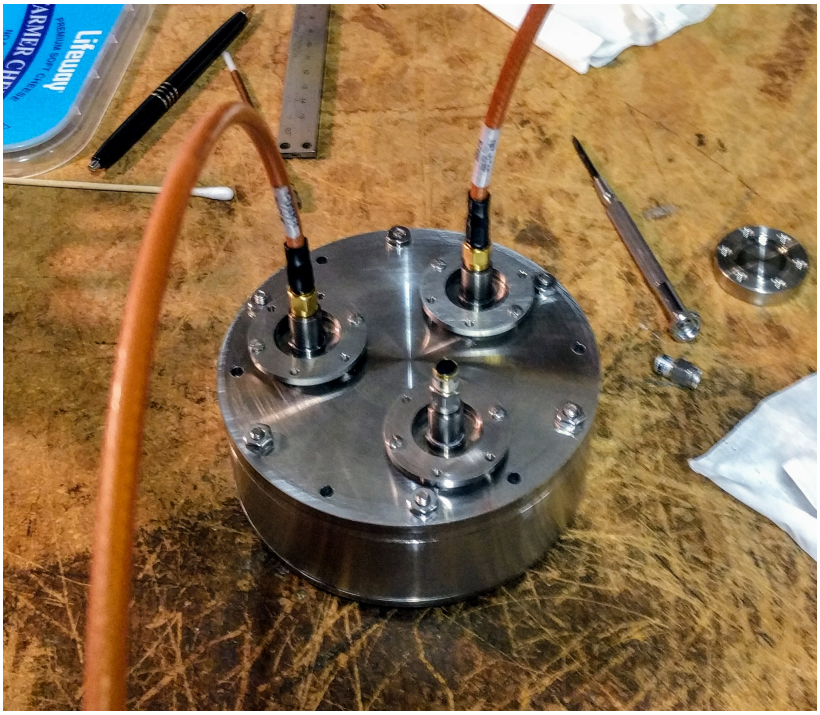

Figure 15. Tunable Q-factor Radio-Frequency cavity.

The experimental test bench utilizes a network analyzer in order to study the variation of the bandwidth around

the resonant frequency of the RF cavity. The loading loops inside the cavity are rotated in order to apply more coupling strength and tune the quality factor. The measurement is performed systematically in 10 degrees rotation increments while recording the matching impedances, loaded Q-factor, and computing the resultant resonant Q-factor. The network analyzer is capable of performing a loaded quality factor calculation that in turn allows to estimate the Q of the cavity. Currently, multiple different coupling loops have been studied which excite the TM resonant mode in a greater or lesser way. The critical coupling of the loops span a quality factor range from $\approx 150-\approx 850$. The results obtained in these measurements are presented below.

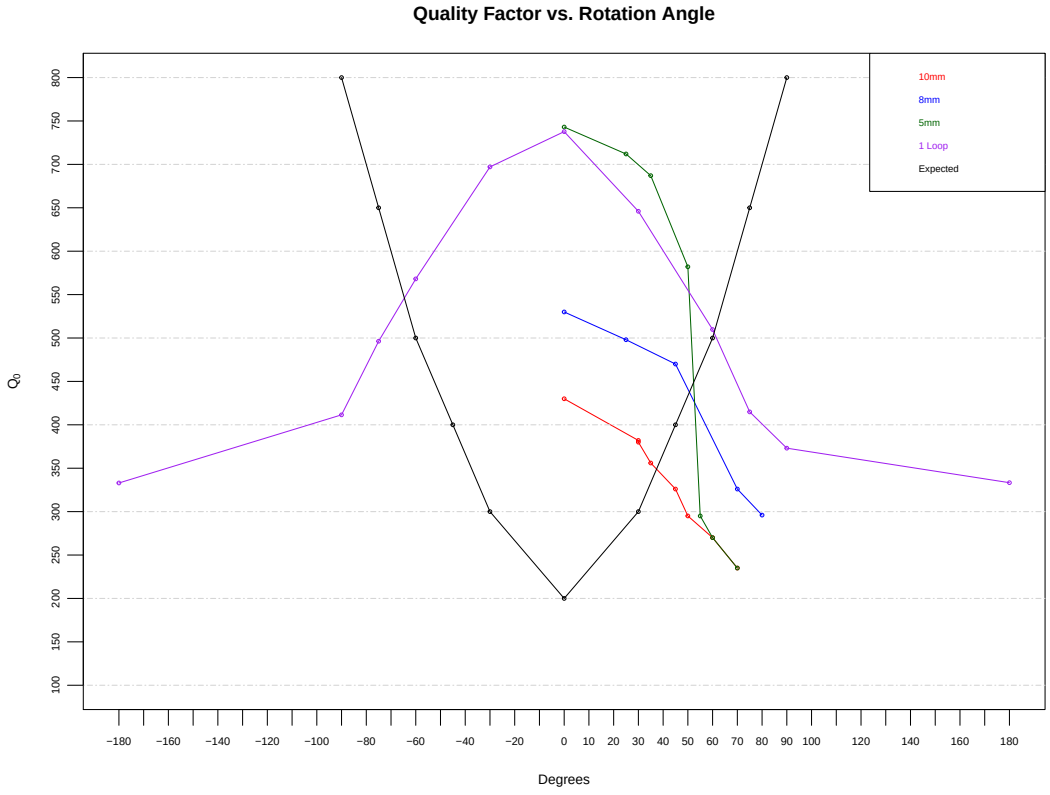

Figure 16. Results plot of measurements of quality factor vs. rotation degree of loading loop.

In the plot above one curve presents a different (and opposite) behavior than the rest – the curve of the expected results. Based on the theoretical behavior of the cavity, when the coupling loops are located at 0° radially with respect to the center the coupling with the magnetic field is maximum. The flux area through the loops is completely open and power should be dissipated at the loops impedances. When the loops are rotated at 90°, however, the coupling was expected to be minimum, as the flux area is not facing the magnetic field and thus there is no power dissipation at the loads. Nevertheless, the results plot presented above shows a completely opposite behavior. Thus, in the first set of benchtop measurements two important conclusions can be drawn: 1) The rotation of the magnetic coupling loops is capable of changing the Q-factor of the cavity throughout the predicted range. 2) The Q-factor of the cavity changes with an opposite behavior than the one predicted by theory.

In the first set of measurements the greatest quality factor was always achieved at 0° when the coupling loops were alligned in a radial direction. Alternatively, the maximum power loss and lowest Q-factor was unexpectedly observed at 90°. Multiple explanations were proposed for this phenomenon, including coupling with undesired modes and breaking of symmetry between the electric field excitation loops around the cavity. In order to study the behavior of the cavity further, a second set of measurements were obtained. In this set the loops were kept at constant angles while the physical size of the loop was changed. Once again, the quality factor was determines by measuring matching impedances, loaded Q-factor, bandwidth, and resonant frequency.

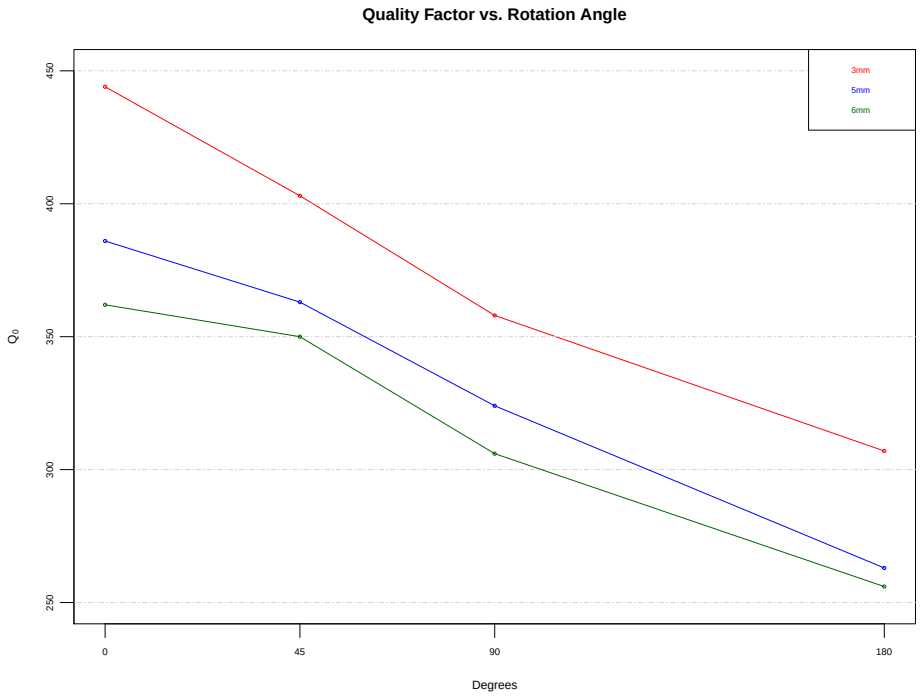

Figure 17. Results plot of measurements of quality factor vs. rotation angle for three different sizes of loop: $3mm, 5mm, 6mm$.

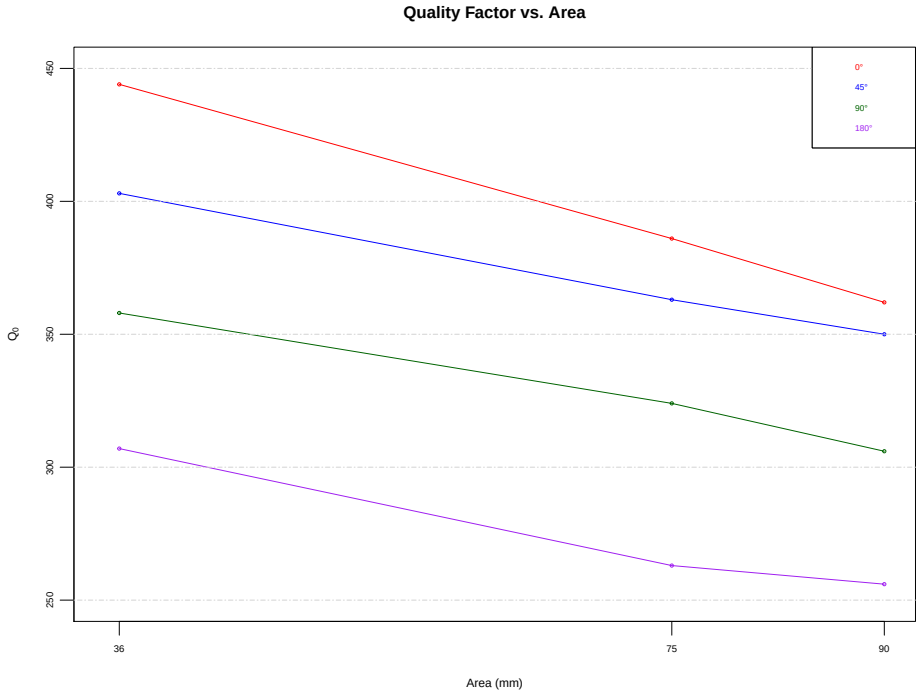

Figure 18. Results plot of measurements of quality factor vs. loading loop aread for three different sizes of loop: $3mm, 5mm, 6mm$.

This second set of measurements proved the fundamental concept behind the tunable Q-factor RF cavity. A greater magnetic flux area dissipates more power in the loading loops, while a smaller flux area has less magnetic coupling and does not dissipate very much power. In the graph shown above, degrees are in presented in the abscissa while

Q-factor is shown in the the ordinate axis. A clear trend can be appreciated here, one that at each angular location smaller loops produce higher Q-factor, while bigger loops dissipate more power and thus have lower Q-factor. This Q-factor result was also plotted as a function of loop area. In the graph shown below, each curve represents an angular measurement swept by different loop areas. In this plot the trend and behavior of the cavity can be more clearly appreciated, in which the Q-factor decreases linearly with flux area.

Throughout the realization of the benchtop measurements for the tunable Q-factor RF cavity, the fundamental concept behind the tunability of the quality factor was proven. Independentely from the rotation angle of the loading loops, smaller loops result in higher quality factor while bigger loops have an opposite effect. The initial design of the RF cavity used the rotation of loops to adjust the variability of magnetic flux area. Nevertheless, the opposite behavior observed in the experimental benchtop measurements ask for a theoretical explanation. Propsed hypotheses include the excitation of undesired modes by rotation of the loops.

An improved designed was proposed for the cavity. In the new design the loading loops are installed around the body of the cavity instead of on the top. This modification will equally allow to modify the magnetic flux area by rotation of the loops. However, in the new design the tunability of the Q would be performed by vertically decreasing the flux area while maintaining the same flux lines through the loop. This might be an important upgrade if symmetry breaking of the E-field excitation in the cavity is a contributing factor to its puzzling behavior observed during the benchtop calibration measurements.

VII. CONCLUDING REMARKS

This analytical and experimental study focused on attaining a better understanding of the proposed RF Cavity Beam Profile Monitor to be used in the Long Baseline Neutrino Facility at Fermilab. This novel beam monitoring system promises to solve many of the problems faced in the NuMI experiment ionizing chamber. Including radiation damage, inefficient pixel configuration, and lack of calibration capability. The traversing beam ionizes gas particles inside the RF cavity which in turn consume the RF power, this power consumption is then proportional to the beam intensity. In order to find the appropriate RF cavity configuration for hadron monitoring applications, several key factors must be obtained: an efficient pixel configuration across the monitor such that the cavities are as sensitive as possible to beam spatial displacements, the magnitude of the electric potential induced by the plasma particles inside the cavity, and the right Q-factor such that precise measurements in high beam intensity can be made. Within this context, the main scientific contribution of this study is to give an initial analysis of all of these factors. This was accomplished analitically by calculating the beam distribution and ion production as well as determining an efficient monitor configuration, and experimentally by using a tunable Q-factor RF cavity in order to find the appropriate gain-to-loss power ratio of the cavity. Future development of the RF Cavity beam profile monitoring system include beam tests of varying intesities at Fermilab facilities.